ACS APPLIED POLYMER MATERIALS

pubs.acs.org/acsapm Article

Frontal Polymerization in Short-Fiber-Reinforced Thermoset Composites

Tolga Topkaya,*,‖ Yuan Gao,‖ and Philippe H. Geubelle

Cite This: https://doi.org/10.1021/acsapm.2c00818 Read Online

ACCESS | Metrics & More | Article Recommendations

ABSTRACT: Frontal polymerization (FP) has recently been introduced as a faster, more energy-efficient manufacturing process for high-performance thermoset composites. This numerical study focuses on the FP-based manufacturing of short-fiber-reinforced polymeric matrix composites. The investigation involves a combination of multiphysics finite element analyses and analytical predictions. The developed model is also applied to a short-fiber composite with spatially varying fiber orientation obtained from a sample produced by vacuum injection method. The results show how the steady-state front velocity and inclination angle depend on the fiber orientation angle and volume fraction. Analytical expressions are derived to capture that dependence and show excellent agreement with the numerical steady-state results. Simulations of FP in short-fiber composites based on experimental distributions of the fiber orientation indicate the feasibility of FP in samples prepared by injection molding.

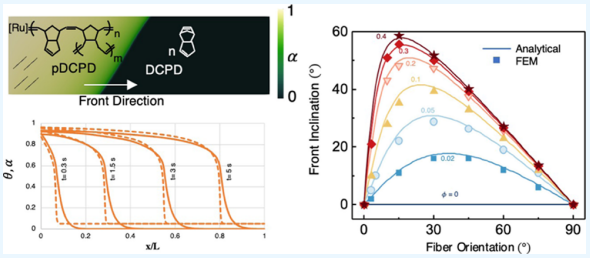

KEYWORDS: *frontal polymerization, short-fiber-reinforced composite, carbon fiber, finite element analysis, dicyclopentadiene*

INTRODUCTION

Thermosetting−polymer−matrix composites are used in a wide variety of engineering applications owing to their excellent mechanical properties and environmental resistance.[1−3] Short-fiber-reinforced polymer (SFRP) composite materials are often the preferred option in many applications, especially automotive, due to their relative ease of production, lower cost, and ability to incorporate different fiber types.[4−9]

The most widely used method to produce SFRP composites, the vacuum injection process, is typically followed by the bulk polymerization of the resin. The present study investigates a different approach for the curing process of SFRP based on the frontal polymerization (FP) of the resin. Introduced in the 1960s,[10] FP consists of a self-propagating exothermic reaction[11,12] usually triggered by a local thermal stimulus.[13,14] It has been observed in a variety of thermosetting polymers characterized by a highly exothermic polymerization reaction and low thermal diffusivity.[15−17]

In addition to the heat of reaction associated with the resin, the thermal properties of the reinforcement material play an important role in determining the characteristic features of FP, that is, the front velocity and shape[18−20]. In continuous-fiber-reinforced polymer (CFRP) composites, reinforcements with high thermal diffusivity, such as carbon or metal fibers, tend to increase the front velocity at low values of the fiber volume fraction.[16,21] However, as the volume fraction of the reinforcing fibers increases, the reduced availability of heat of reaction as the resin volume fraction decreases leads to a reduction in the front speed.[22] As shown by Vyas et al.,[23] this non-monotonic dependence of the front speed on the fiber volume fraction is not present in unidirectional glass-fiber CFRP composites due to the lower thermal diffusivity of the fibers.

Goli et al. and Vyas et al. have developed homogenized reaction-diffusion models for FP in unidirectional composites with continuous carbon and glass fibers.[22,23] Based on the homogenized model, Kumar et al. derived an analytical expression of the front velocity that includes the effect of the fiber volume fraction, the homogenized thermal properties of the composite material, and the parameters that define the cure kinetics of the resin.[24] More recently, Wang has investigated the effect of microstructures on the through-thickness frontal polymerization in unidirectional carbon−fiber composites with the reaction-diffusion model.[25] The homogenized reaction-diffusion model was also used by Goli et al. to study FP-driven instabilities in carbon−dicyclopentadiene (DCPD) composites.[26] Also relevant to the modeling of polymerization front

Received: May 13, 2022
Accepted: August 26, 2022

Table 1. Thermal Properties and Cure Kinetics Parameters of DCPD Resin[24]

κ_r(W/m·K)	$\rho_r\left(\frac{kg}{m^3}\right)$	Cp_r(J/kg·K)	E(kJ/mol)	A(1/s)	n	m	C	α_c	H_r(J/g)
0.15	980	1600	110.75	8.55 × 1015	1.72	0.77	14.48	0.41	350

propagation in fiber-reinforced composites are the simulations performed by Gao et al. of FP in model composites with thermally conductive materials and in transversely isotropic composites.[19,27] While these previous studies pertained to the simulation of frontal polymerization in continuous-fiber-reinforced composites with the fibers aligned in the direction of the front propagation, the present work focuses on short-fiber-reinforced composites with an arbitrary orientation of the reinforcing phase.

The key objective of the present study is to investigate the applicability of FP to the manufacturing of SFRP and in particular to study how the short-fiber volume fraction and orientation affect the propagation of the front. The present work is motivated by the study by Chen and Wang, who showed that thermal conductivity of SFRP composites is strongly connected to fiber type.[28] The preliminary numerical and analytical study presented hereafter focuses on SFRP composites made of carbon fibers and DCPD resin. While the analysis focuses on FP in planar (2D) SFRP composite parts, this work is also motivated by current efforts to 3D print SFRP composites, where the composite properties are critical to the production rate and quality.[29,30]

In the present study, we investigate FP in SFRP composites using a multiphysics finite element solver based on a homogenized thermo-chemical model. The homogenized anisotropic thermal properties of SFRP are described by the Halpin−Tsai model. The results indicate that the impact of the orientation and volume fraction of the short fibers on the heat conduction of the composite leads to variations in both front velocity and inclination angle. Analytical descriptions of the front velocity and inclination angle are also developed and verified with the aid of a detailed parametric study. Finally, the developed thermo-chemical model is applied to simulate FP in components with spatially varying fiber orientations such as those found in samples produced by vacuum-injection molding.

The article is organized as follows: Section 2 summarizes the model formulation and describes the problem used to simulate FP in SFRP composites. The numerical results are compared with analytical predictions of the front angle and speed in Section 3, which also contains the simulation of FP in an SFRP composite made through vacuum-injection molding, based on fiber orientations inspired by those extracted experimentally by Thi et al.[31]

PROBLEM FORMULATION

FP in SFRP composites with DCPD resin (denoted by the subscript "r") and short fibers (denoted by the subscript "f") with a volume fraction ϕ is described by the following reaction-diffusion partial differential equations (PDEs)[23]

$$\begin{cases} \rho_r H_r \frac{\partial \alpha}{\partial t}(1-\phi) + \frac{\partial}{\partial x_i}\left(\overline{\kappa_{ij}}\frac{\partial T}{\partial x_j}\right) = \overline{\rho C_p}\frac{\partial T}{\partial t}, \\ \frac{\partial \alpha}{\partial t} = A\exp\left(\frac{-E}{RT}\right)(1-\alpha)^n \alpha^m \frac{1}{1+\exp[C(\alpha-\alpha_c)]} \end{cases} \quad (1)$$

In the first relation, T and α, respectively, denote the dependent variables of this nonlinear, coupled problem, that is, the temperature (in K) and the degree of cure (non-dimensional); t (in s) denotes time; ρ_r (in kg/m^3) and H_r (in J/kg), respectively, represent the density and heat of reaction of the resin; and $\overline{\kappa_{ij}}$ (in W/m K) denotes the homogenized thermal conductivity matrix of the composite, with the subscripts i, j taking the values 1 and 2 in this 2D study. The degree of cure describes the fractional conversion of the polymerization based on the reaction heat and can be measured with differential scanning calorimetry.[32] The homogenized expression $\overline{\rho C_p}$ is obtained through the rule of mixture as

$$\overline{\rho C_p} = \rho_r C_{pr}(1-\phi) + \rho_f C_{pf}\phi \quad (2)$$

where C_p (in J/kg K) and ρ (in kg/m^3) denote the heat capacity and density, respectively. In our study, the volume fraction of short fibers ϕ ranges between 0 and 0.4.

To study the FP in SFRC with various fiber orientations, the Halpin−Tsai model[33−35] is adopted hereafter to evaluate the anisotropic homogenized thermal conductivities $\overline{\kappa_{ij}}$ of the SFRP composite

$$\overline{\kappa_{ij}} = \begin{Bmatrix} \overline{\kappa_{11}} & \overline{\kappa_{12}} \\ \overline{\kappa_{21}} & \overline{\kappa_{22}} \end{Bmatrix} = \begin{Bmatrix} \cos^2\beta\,\overline{\kappa_{\parallel}} + \sin^2\beta\,\overline{\kappa_{\perp}} & \cos\beta\sin\beta(\overline{\kappa_{\parallel}} - \overline{\kappa_{\perp}}) \\ \cos\beta\sin\beta(\overline{\kappa_{\parallel}} - \overline{\kappa_{\perp}}) & \sin^2\beta\,\overline{\kappa_{\parallel}} + \cos^2\beta\,\overline{\kappa_{\perp}} \end{Bmatrix} \quad (3)$$

where β is the orientation of the fibers and ranges between 0 and 90°. In eq 3, $\kappa_{\parallel}$ and $\kappa_{\perp}$, respectively, denote the thermal conductivity of the SFRP composite in directions parallel and perpendicular to the fiber orientation obtained by

$$\kappa_{\parallel} = \frac{1+(l_f/d)\mu_1\phi}{1-\mu_1\phi}\kappa_r, \quad \kappa_{\perp} = \frac{1+2\mu_2\phi}{1-\mu_2\phi}\kappa_r$$
$$\mu_1 = \frac{\kappa_{f1}/\kappa_r - 1}{\kappa_{f1}/\kappa_r + 2l_f/d}, \quad \mu_2 = \frac{\kappa_{f2}/\kappa_r - 1}{\kappa_{f2}/\kappa_r + 2} \quad (4)$$

In these expressions, κ_{f1}, κ_{f2}, and κ_r (all in W/m K), respectively, denote the thermal conductivity of carbon fibers parallel and perpendicular to the fiber axis and the thermal conductivity of DCPD. The aspect ratio of fibers $\frac{l_f}{d}$ is chosen hereafter to be 100, with l_f and d, respectively, representing the length and diameter of fibers.

The second relation in eq 1 describes the cure kinetics model, with H_r (in J/kg), A (in 1/s), E (in J/mol), and R (=8.314 J/mol K) denoting the heat of reaction, pre-exponential factor, activation energy, and ideal gas constant, respectively. The cure kinetics can capture the effect of cross-linking.[36] The thermal properties and cure kinetics parameters of the DCPD resin are summarized in Table 1, and the physical properties of the short fibers are given in Table 2. All material properties were assumed to be constant during polymerization.

https://doi.org/10.1021/acsapm.2c00818
ACS Appl. Polym. Mater. XXXX, XXX, XXX−XXX

Table 2. Physical Properties of the Short Carbon Fiber[37]

κ_{f1}(W/m·K)	κ_{f2}(W/m·K)	Cp_f(J/kg·K)	$\rho_f\left(\frac{kg}{m^3}\right)$	$\frac{l_f}{d}$
9.3	0.67	753.6	1800	100

The governing PDEs are solved with the following initial and boundary conditions

$$\begin{cases} T(x_1, x_2, 0) = T_0, \\ \alpha(x_1, x_2, 0) = \alpha_0, \\ T(0, x_2, t) = T_{trig} \text{ for } 0 \le t \le t_{trig}, \\ \frac{\partial T}{\partial x_1}(0, x_2, t) = 0 \text{ for } t > t_{trig} \end{cases} \quad (5)$$

The initial temperature T_0 and degree of cure α_0 are set as 20 °C and 0.05, respectively. To initiate the frontal polymerization, a triggering temperature T_{trig} = 200 °C is applied along the left boundary of the domain for t_{trig} = 1 s. Adiabatic boundary conditions are adopted along the other boundaries. The governing equations along with the initial and boundary conditions were solved in a 2D rectangular domain with a length l = 10 mm and a width w = 3 mm (Figure 1).

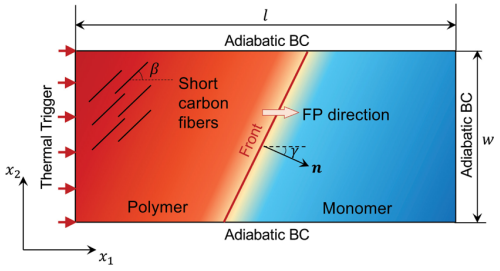

Figure 1. Schematic of the 2D rectangular numerical domain of length l and width w. Fiber orientation angle and front inclination angle are defined as β and γ, respectively. The fiber volume fraction is named ϕ and ranges between 0 and 0.4. The front was initiated by a Dirichlet boundary condition at the left boundary, indicated by the red arrows. Adiabatic boundary conditions were applied at other boundaries.

The simulations are performed using the Multiphysics Object-Oriented Simulation Environment[38] for its ability to capture the sharp gradients in temperature T and degree-of-cure α profiles in the vicinity of the propagating front with the aid of mesh and time-step adaptivity modules.

In the remainder of the document, the temperature solution is usually presented in a non-dimensional form as

$$\theta = \frac{T - T_0}{T_f - T_0} = \frac{(T - T_0)\overline{\rho C_p}}{\rho_r H_r (1 - \alpha_0)(1 - \phi)} \quad (6)$$

where T_f denotes the adiabatic temperature of the front defined as

$$T_f = T_0 + \frac{\rho_r H_r (1 - \alpha_0)(1 - \phi)}{\overline{\rho C_p}} \quad (7)$$

3. RESULTS AND DISCUSSION

3.1. Typical Results. Typical numerical solutions obtained with β = 30° and ϕ = 0.2 are shown in Figure 2, which presents snapshots of the temperature T (Figure 2a) and degree-of-cure α (Figure 2b) fields at times t_1 = 0.5 s, t_2 = 2.0 s, and t_3 = 6.0 s. After the initial transients associated with the initiation of the polymerization front along the left edge of the domain (t_1 = 0.5 s), the polymerization front adopts a straight, inclined, and steady-state shape to reflect the anisotropic heat conduction associated with the presence of the short fibers. Figure 2c shows the 1D profiles of α and θ at t_1, t_2, and t_3. The thermal front (identified by θ = 0.5) and the chemical front (identified by α = 0.5) propagate simultaneously, with the thermal front leading the chemical front.

Figure 2d presents the evolution of the front location in the x_1-direction, x_f, along the top (x_2 = 3 mm), in the middle (x_2 = 1.5 mm), and along the bottom (x_2 = 0 mm) of the numerical domain. After t_2 = 2 s, the results indicate a steady-state regime with constant front velocity and inclination angle. The acceleration of front observed beyond t_3 = 6 s is associated with the boundary effect. All results for the front inclination angle and velocity presented hereafter are obtained within the steady-state regime.

3.2. Front Inclination. Building on the observations presented in Section 3.1, we perform hereafter a parametric

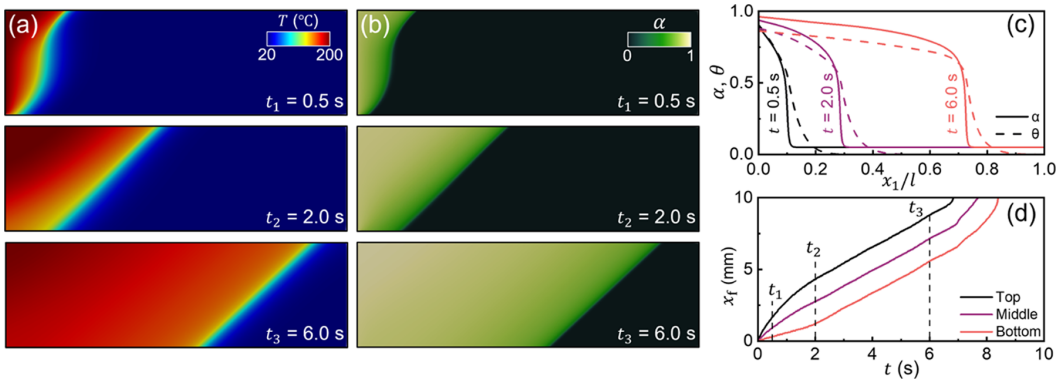

Figure 2. Typical numerical results for β = 30° and ϕ = 0.2. Numerical snapshots of (a) temperature T and (b) degree of cure α at t_1 = 0.5 s, t_2 = 2.0 s, and t_3 = 6.0 s. (c) 1D profiles of degree of cure α and normalized temperature θ in the middle of the domain (x_2 = 1.5 mm). (d) Front displacement x_f as a function of time t along the top (x_2 = 3 mm), in the middle (x_2 = 1.5 mm), and along the bottom (x_2 = 0 mm) of the numerical domain.

https://doi.org/10.1021/acsapm.2c00818
ACS Appl. Polym. Mater. XXXX, XXX, XXX−XXX

study of the effects of the orientation angle β and volume fraction of short fibers ϕ on the inclination angle γ of the front. Figures 3a,b, respectively, shows the steady-state fronts

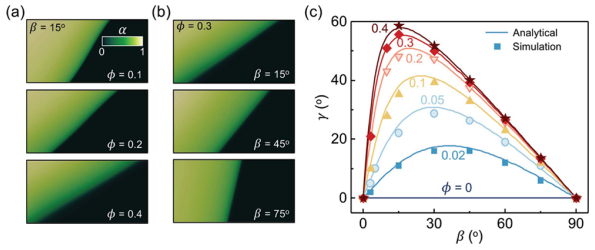

Figure 3. Effect of fiber orientation β and volume fraction ϕ on the front inclination in steady-state regime. Numerical snapshots of degree-of-cure α distributions obtained for (a) $\beta = 15°$ and $\phi = 0.1$, 0.2, and 0.4 and (b) $\phi = 0.3$ and $\beta = 15$, 45, and 75°. (c) γ *vs* β for different values of ϕ. The solid curves and symbols, respectively, represent analytical expression in eq 11 and numerical results.

obtained for various values of ϕ and γ. As apparent in Figure 3a, the front angle γ increases with ϕ for a fixed value of the fiber orientation $\beta = 15°$. Conversely, for a constant value of $\phi = 0.3$, γ decreases with increasing values of β. However, as apparent in Figure 3c, which presents a summary of all numerical simulations (shown as symbols), the dependence of γ on β is non-monotonic, with the value of β corresponding to the maximum front inclination angle reducing with increasing ϕ.

An analytical expression of γ as a function of β and ϕ can be derived, starting with the expression of the x_1 and x_2 component of the heat flux

$$\begin{cases} q_{x_1} = -\overline{\kappa_{11}}\frac{\partial T}{\partial x_1} - \overline{\kappa_{12}}\frac{\partial T}{\partial x_2} \\ q_{x_2} = -\overline{\kappa_{12}}\frac{\partial T}{\partial x_1} - \overline{\kappa_{22}}\frac{\partial T}{\partial x_2} \end{cases} \tag{8}$$

Imposing a zero value of the normal heat flux along the adiabatic top and bottom edges leads to

$$-\overline{\kappa_{12}}\frac{\partial T}{\partial x_1} - \overline{\kappa_{22}}\frac{\partial T}{\partial x_2} = 0 \tag{9}$$

Along the propagating front, the tangential component of the heat flux vanishes, which yields

$$\frac{\partial T}{\partial x_1}\sin\gamma + \frac{\partial T}{\partial x_2}\cos\gamma = 0 \tag{10}$$

Combining (9) and (10) leads to

$$\gamma = \tan^{-1}\frac{\overline{\kappa_{12}}}{\overline{\kappa_{22}}} \tag{11}$$

As shown in Figure 3c, the analytical expression (11) of the steady-state front angle matches very well the numerically extracted values.

3.3. Front Velocity. Figure 4a shows the front location x_f in the middle of the domain ($x_2 = 1.5$ mm) as a function of time t with various fiber orientation angles β. The initial trajectory of the front is the same for all four values of ϕ, as it is influenced by the thermal trigger. After reaching $x_f \approx 2$ mm, the front enters its quasi-steady-state propagation regime, with a speed v_f (i.e., the slope of the x_f–t curve) decreasing with increasing values of ϕ. As indicated earlier, the reduction in v_f

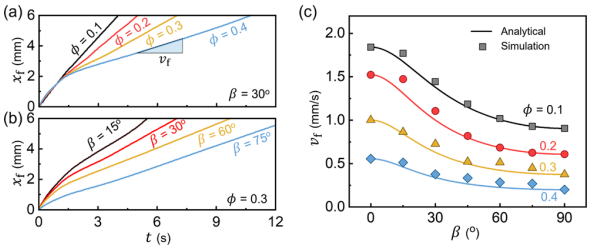

Figure 4. Extraction of the polymerization front velocity. Front location x_f as a function of time t for (a) $\beta = 30°$ and $\phi = 0.1$, 0.2, 0.3, and 0.4 and (b) $\phi = 0.3$ and $\beta = 15$, 30, 60, and 75°. (c) β-dependence of the front velocity v_f for four values of ϕ. The curves and symbols, respectively, represent the analytical expression (13) and the numerical results.

with increasing ϕ is due to the relative decrease in the amount of resin and thereby of the amount of exothermic heat of reaction. Figure 4b presents the x_f–t curves obtained for different fiber orientation angles β. As apparent there, it takes longer for the front progression to reach steady state for lower fiber orientation angles and the front velocity v_f is higher.

The dependence of v_f on both β and ϕ can also be derived analytically, starting from the following asymptotic expression of the front velocity in a thermally isotropic homogenized resin derived by Kumar et al.[24]

$$V_f = \max_{\epsilon}\left[\frac{A_r\overline{\kappa}}{\rho_r H_r(1-\phi)\rho_f\phi}\frac{R\hat{T}(\epsilon)^2}{E_r}\exp\left(\frac{-Em}{R\hat{T}(\epsilon)}\right)\frac{1}{\Pi[m, n, C, \alpha_c, \alpha_0, \epsilon]}\right]^{0.5} \tag{12}$$

where $\hat{T}(\epsilon) = T_0 + \frac{(1-\phi)(1-\alpha_0-\epsilon)\rho_r H_r}{\overline{\rho C_p}}$, ϵ is between 0 and $1-\alpha_0$, $\overline{\kappa}$ is the isotropic homogenized thermal conductivity, and $\Pi[m, n, C, \alpha_c\alpha_0, \epsilon]$

$$= \int_0^{1-\epsilon-\alpha_0}\frac{y}{(y+\epsilon)^n(1-\epsilon-y)^m}(1+\exp(C(1-\epsilon-\alpha_c-y)))\mathrm{d}y$$

Equation 12 can be used to predict the front velocity parallel ($\beta = 0°$) $v_{f\|}$ and perpendicular ($\beta = 90°$) $v_{f\perp}$ to the fiber orientation by substituting $\overline{\kappa}$ with $\kappa_\|$ and $\kappa_\perp$ defined in 4. For β values other than $\beta = 0°$ and $\beta = 90°$, the analytical prediction relies on the relation between $v_f(\beta)$, $v_{f\|}$, and $v_{f\perp}$ as

$$v_f(\beta) = \sqrt{\frac{(v_{f\|}v_{f\perp})^2(1+\tan^2\beta)}{v_{f\|}^2\tan^2\beta + v_{f\perp}^2}} \tag{13}$$

The analytical expression (13) is plotted as a set of solid curves in Figure 4c and shows very good agreement with simulation results (shown as symbols) for all four values of the fiber volume fraction.

Based on the theoretical expressions in eqs 12 and 13, we present in Figure 5 the dependence of the front velocity v_f on the fiber aspect ratio $\frac{l_f}{d}$ with $\phi = 0.2$ (Figure 5). Over the typical range $50 \le \frac{l_f}{d} \le 1000$,[28,39] v_f increases from 1.41 to 1.66 mm/s for $\beta = 0°$ (black curve). For a higher value of β, the $v_f - \frac{l_f}{d}$ dependence is weaker but remains positive (red, yellow, and blue curves).

https://doi.org/10.1021/acsapm.2c00818
ACS Appl. Polym. Mater. XXXX, XXX, XXX−XXX

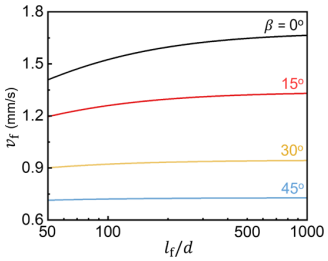

Figure 5. Front velocity v_f as a function of short fiber aspect ratio $\frac{l_f}{d}$ with fiber volume fraction ϕ = 0.2. Four values of fiber orientation angle β = 0, 15, 30, and 45° are considered.

3.4. Illustration: FP in Vacuum Injection-Molded SFRP Composites. In this section, we apply the homogenized thermo-chemical model to the simulation of FP in a typical SFRP composite produced by vacuum injection molding, for which the orientation β is heterogeneous across the sample. In the absence of experimental data on the vacuum-injection-generated distribution of fiber orientation in the carbon−DCPD SFRP composite, we adopt in this illustrative study the fiber orientation distributions extracted in a previous work[31] using tensor notation[40,41] at three locations (labeled A, B, and C) of a vacuum-injection-molded 6T-860 (PA6) SFRP composite part, with points A and C, respectively, located the closest to and furthest from the injection point.

Based on the fiber orientation measurements provided by Thi et al.,[31] we adopt the three through-thickness β distributions shown in Figure 6a, with $0 \leq x_3 \leq 3$ mm denoting the coordinate across the thickness of the composite part. As apparent there, the β distribution is symmetric with respect to the mid-thickness plane x_3 = 1.5 mm. Fiber orientation angles vary between 12 and 18.75° for distribution A, between 15.5 and 20.81° for distribution B, and between 10.52 and 15.38° for distribution C. The fiber volume fraction ϕ is set as 48% as indicated in ref 31. As previously, adiabatic conditions are applied along the top and bottom edges of the domain.

Figure 6b shows snapshots of temperature T (top contours) and degree-of-cure α (bottom contours) fields obtained during the propagation of the polymerization front in homogenized SFRP materials described by fiber orientation distributions A, B, and C. For all three cases, the symmetric distribution of β drives the reaction heat to the middle of the system, forming a triangular shape, with the leading edge of the front located along the symmetry plane. The front shapes are similar due to the relatively small variation range of β (10.52−20.81°). The front temperature T_f is 141.6 °C, agreeing quite well with the analytical expression for systems with homogeneous β distribution in eq 7, which yields 135.5 °C. Figure 6c displays the steady-state front velocity values for the three distributions. The front velocity is ∼0.51 mm/s, slightly higher than the theoretical prediction based on homogeneous β by eqs 12 and 13, which yields 0.37 (20°)∼0.45 mm/s (10°).

4. CONCLUSIONS

We have numerically and theoretically investigated the frontal-polymerization-based manufacturing of short-fiber-reinforced thermoset polymer composites, with emphasis on a carbon/DCPD system. The study has focused on the development and implementation of a homogenized thermo-chemical model to capture the initiation and propagation of the polymerization front and on the analysis of the impact of the fiber orientation and volume fraction on the steady-state shape, orientation, and velocity of the front. The finite element simulations have shown that, after a transient period associated with the initiation of the frontal polymerization process, the front adopts a straight profile inclined with respect to the propagation direction. The numerical and theoretical analyses have demonstrated a strong dependence of the inclination angle of the front on the orientation and volume fraction of the short fibers, with the highest sensitivity obtained for higher volume fraction values. Numerically extracted values of the steady-state front velocity have been shown to decrease monotonically with both the fiber orientation and volume fraction. A closed-form expression of that dependence was derived based on theoretical predictions of the front velocity in directions parallel and perpendicular to the fiber directions, and excellent agreement has been found between numerical and analytical results.

Building on these results, we have investigated the propagation of a polymerization front in composite materials with fiber orientation varying across the thickness. The three

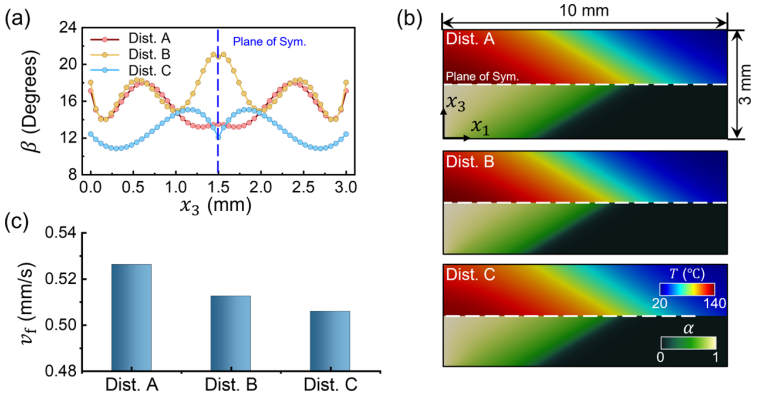

Figure 6. FP in SFRP with three spatially varying fiber orientations inspired by measurements conducted on a composite part produced by vacuum injection molding.[31] (a) Fiber orientation distributions (labeled A, B, and C) across the thickness of the specimen. The distributions of fiber orientations are symmetric with respect to the plane x_3 = 1.5 mm. (b) Temperature T and degree-of-cure α contours obtained at time t = 4 s. (c) Front velocities v_f.

https://doi.org/10.1021/acsapm.2c00818
ACS Appl. Polym. Mater. XXXX, XXX, XXX−XXX

fiber orientation distributions used in that study have been inspired by experimental observations obtained by Thi et al.[31] for an SFRP composite produced by vacuum injection molding. The numerical results have yielded relatively small variations in the front shape and speed between the three fiber orientation distributions. Moreover, all orientation distributions investigated in this study lead to a stable front propagation, which will likely ensure the quality of the composite product. These features point to the applicability of FP-based manufacturing of SFRP composites.

AUTHOR INFORMATION

Corresponding Author

Tolga Topkaya − *Department of Mechanical Engineering, Batman University, Batman 72060, Turkey; Beckman Institute of Advanced Science and Technology, University of Illinois, Urbana 61801, United States; Department of Aerospace Engineering, University of Illinois, Urbana, Illinois 61801, United States;* orcid.org/0000-0001-6650-8067; Email: tolga.topkaya@batman.edu.tr

Authors

Yuan Gao − *Beckman Institute of Advanced Science and Technology, University of Illinois, Urbana 61801, United States; Department of Aerospace Engineering, University of Illinois, Urbana, Illinois 61801, United States;* orcid.org/0000-0001-6030-9497

Philippe H. Geubelle − *Beckman Institute of Advanced Science and Technology, University of Illinois, Urbana 61801, United States; Department of Aerospace Engineering, University of Illinois, Urbana, Illinois 61801, United States;* orcid.org/0000-0002-4670-5474

Complete contact information is available at: https://pubs.acs.org/10.1021/acsapm.2c00818

Author Contributions

‖T.T. and Y.G. contributed equally.

Notes

The authors declare no competing financial interest.

ACKNOWLEDGMENTS

Dr. Tolga TOPKAYA acknowledges financial support from the Scientific and Technological Research Council of Turkey (TUBITAK) BIDEB-2219 International Postdoctoral Research Programme (app. no: 1059B191900205) during his sabbatical stay at the Beckman Institute at the University of Illinois. The authors acknowledge the support of the National Science Foundation for grant no. 1933932 through the GOALI: Manufacturing USA: Energy Efficient Processing of Thermosetting Polymers and Composites, with additional support from the U.S. Air Force Office of Scientific Research through award FA9550-20-1-0194 as part of the Center of Excellence in Self-healing and Morphogenic Manufacturing.

REFERENCES

(1) Pascault, J.; Sautereau, H.; Verdu, J.; Williams, R. *Thermosetting Polymers*; CRC press, 2002; Vol. *64*.

(2) Daniel, I.; Ishai, O. *Engineering Mechanics of Composite Materials*; Oxford University Press: New York, 1994; Vol. *3*.

(3) Brøndsted, P.; Lilholt, H.; Lystrup, A. Composite Materials for Wind Power Turbine Blades. *Annu. Rev. Mater. Res.* **2005**, *35*, 505−538.

(4) Fernandes, C.; Pontes, A. J.; Viana, J. C.; Gaspar-Cunha, A. Modeling and optimization of the injection-molding process: A Review. *Adv. Polym. Technol.* **2018**, *37*, 429−449.

(5) Naili, C.; Doghri, I.; Kanit, T.; Sukiman, M.; Aissa-Berraies, A.; Imad, A. Short fiber reinforced composites: Unbiased full-field evaluation of various homogenization methods in elasticity. *Compos. Sci. Technol.* **2020**, *187*, 107942.

(6) Zarges, J.-C.; Sälzer, P.; Heim, H.-P. Correlation of fiber orientation and fiber-matrix-interaction of injection-molded polypropylene cellulose fiber composites. *Composites, Part A* **2020**, *139*, 106112.

(7) Proy, J.; Massa, F.; Notta-Cuvier, D.; Lauro, F.; Tison, T.; Spingler, G. Integrating fibers and injection molding process variability in short-natural-fiber-reinforced thermoplastics behavior: A review. *Mater. Today Commun.* **2021**, *29*, 102785.

(8) Mortazavian, S.; Fatemi, A. Effects of fiber orientation and anisotropy on tensile strength and elastic modulus of short fiber reinforced polymer composites. *Composites, Part B* **2015**, *72*, 116−129.

(9) Arao, Y.; Fujiura, T.; Itani, S.; Tanaka, T. Strength improvement in injection-molded jute-fiber-reinforced polylactide green-composites. *Composites, Part B* **2015**, *68*, 200−206.

(10) Pshezhetskii, V. S.; Tupikov, V. I. *Geterotsepnye Vysokomolekulyarnye Soedineniya (Heterochain High-Molecular-Mass Compounds)*; Nauka: Moscow, 1963.

(11) Ruiu, A.; Sanna, D.; Alzari, V.; Nuvoli, D.; Mariani, A. Advances in the frontal ring opening metathesis polymerization of dicyclopentadiene. *J. Polym. Sci., Part A: Polym. Chem.* **2014**, *52*, 2776−2780.

(12) Mariani, A.; Fiori, S.; Chekanov, Y.; Pojman, J. A. Frontal ring-opening metathesis polymerization of dicyclopentadiene. *Macromolecules* **2001**, *34*, 6539−6541.

(13) Lloyd, E. M.; Feinberg, E. C.; Gao, Y.; Peterson, S. R.; Soman, B.; Hemmer, J.; Dean, L. M.; Wu, Q.; Geubelle, P. H.; Sottos, N. R.; Moore, J. S. Spontaneous patterning during frontal polymerization. *ACS Cent. Sci.* **2021**, *7*, 603−612.

(14) Goli, E.; Gai, T.; Geubelle, P. Impact of boundary heat losses on frontal polymerization. *J. Phys. Chem. B* **2020**, *124*, 6404−6411.

(15) Groce, B. R.; Gary, D. P.; Cantrell, J. K.; Pojman, J. A. Front velocity dependence on vinyl ether and initiator concentration in radical-induced cationic frontal polymerization of epoxies. *J. Polym. Sci.* **2021**, *59*, 1678−1685.

(16) Vyas, S.; Zhang, X.; Goli, E.; Geubelle, P. Frontal vs. bulk polymerization of fiber-reinforced polymer-matrix composites. *Compos. Sci. Technol.* **2020**, *198*, 108303.

(17) Mariani, A.; Bidali, S.; Fiori, S.; Sangermano, M.; Malucelli, G.; Bongiovanni, R.; Priola, A. UV-ignited frontal polymerization of an epoxy resin. *J. Polym. Sci., Part A: Polym. Chem.* **2004**, *42*, 2066−2072.

(18) Gao, Y.; Dearborn, M. A.; Vyas, S.; Kumar, A.; Hemmer, J.; Wang, Z.; Wu, Q.; Alshangiti, O.; Moore, J. S.; Esser-Kahn, A. P.; Geubelle, P. H. Manipulating frontal polymerization and instabilities with phase-changing microparticles. *J. Phys. Chem. B* **2021**, *125*, 7537−7545.

(19) Gao, Y.; Li, S.; Kim, J.-Y.; Hoffman, I.; Vyas, S. K.; Pojman, J. A.; Geubelle, P. H. Anisotropic frontal polymerization in a model resin-copper composite. *Chaos* **2022**, *32*, 013109.

(20) Gross, L.; Volpert, V. Weakly nonlinear stability analysis of frontal polymerization. *Stud. Appl. Math.* **2003**, *110*, 351−375.

(21) Goli, E.; Robertson, I. D.; Agarwal, H.; Pruitt, E. L.; Grolman, J. M.; Geubelle, P. H.; Moore, J. S. Frontal polymerization accelerated by continuous conductive elements. *J. Appl. Polym. Sci.* **2019**, *136*, 47418.

(22) Goli, E.; Parikh, N.; Yourdkhani, M.; Hibbard, N.; Moore, J.; Sottos, N.; Geubelle, P. Frontal polymerization of unidirectional carbon-fiber-reinforced composites. *Composites, Part A* **2020**, *130*, 105689.

(23) Vyas, S.; Goli, E.; Zhang, X.; Geubelle, P. Manufacturing of unidirectional glass-fiber-reinforced composites via frontal polymerization: A numerical study. *Compos. Sci. Technol.* **2019**, *184*, 107832.

(24) Kumar, A.; Gao, Y.; Geubelle, P. H. Analytical estimates of front velocity in the frontal polymerization of thermoset polymers and composites. *J. Polym. Sci.* **2021**, *59*, 1109−1118.
(25) Wang, Y. Modeling the through-thickness frontal polymerization of unidirectional carbon fiber thermoset composites: Effect of microstructures. *J. Appl. Polym. Sci.* **2022**, *139*, No. e52735.
(26) Goli, E.; Peterson, S. R.; Geubelle, P. H. Instabilities driven by frontal polymerization in thermosetting polymers and composites. *Composites, Part B* **2020**, *199*, 108306.
(27) Gao, Y.; Shaon, F.; Kumar, A.; Bynum, S.; Gary, D.; Sharp, D.; Pojman, J. A.; Geubelle, P. H. Rapid frontal polymerization achieved with thermally conductive metal strips. *Chaos* **2021**, *31*, 073113.
(28) Chen, C.-H.; Wang, Y.-C. Effective thermal conductivity of misoriented short-fiber reinforced thermoplastics. *Mech. Mater.* **1996**, *23*, 217−228.
(29) Zhang, Z.; Liu, R.; Li, W.; Liu, Y.; Pei, Z.; Qiu, J.; Wang, S. Frontal polymerization-assisted 3D printing of short carbon fibers/dicyclopentadiene composites. *J. Manuf. Process.* **2021**, *71*, 753−762.
(30) Park, S.; Shou, W.; Makatura, L.; Matusik, W.; Fu, K. K. 3D printing of polymer composites: Materials, processes, and applications. *Matter* **2022**, *5*, 43−76.
(31) Thi, T. B. N.; Morioka, M.; Yokoyama, A.; Hamanaka, S.; Yamashita, K.; Nonomura, C. Measurement of fiber orientation distribution in injection-molded short-glass-fiber composites using X-ray computed tomography. *J. Mater. Process. Technol.* **2015**, *219*, 1−9.
(32) Yang, G.; Lee, J. Curing Kinetics and Mechanical Properties of endo-Dicyclopentadiene Synthesized Using Different Grubbs' Catalysts. *Ind. Eng. Chem. Res.* **2014**, *53*, 3001−3011.
(33) Halpin, J. C.; Finlayson, K. M. *Primer on Composite Materials Analysis*; Routledge, 2017.
(34) Fu, S.-Y.; Lauke, B.; Mai, Y.-W. *Science and Engineering of Short Fibre-Reinforced Polymer Composites*; Woodhead Publishing, 2019.
(35) Choy, C.; Kwok, K. W.; Leung, W.; Lau, F. P. Thermal conductivity of poly(ether ether ketone) and its short-fiber composites. *J. Polym. Sci., Part B: Polym. Phys.* **1994**, *32*, 1389−1397.
(36) Hennessy, M. G.; Vitale, A.; Cabral, J. T.; Matar, O. K. Role of heat generation and thermal diffusion during frontal photopolymerization. *Phys. Rev. E: Stat., Nonlinear, Soft Matter Phys.* **2015**, *92*, 022403.
(37) Choy, C.; Leung, W.; Kowk, K.; Lau, F. P. Elastic moduli and thermal conductivity of injection-molded short-fiber-reinforced thermoplastics. *Polym. Compos.* **1992**, *13*, 69−80.
(38) Gaston, D.; Newman, C.; Hansen, G.; Lebrun-Grandié, D. MOOSE: A parallel computational framework for coupled systems of nonlinear equations. *Nucl. Eng. Des.* **2009**, *239*, 1768−1778.
(39) Tucker, C. L., III; Liang, E. Stiffness predictions for unidirectional short-fiber composites: review and evaluation. *Compos. Sci. Technol.* **1999**, *59*, 655−671.
(40) Bay, R. S.; Tucker, C. L., III Fiber orientation in simple injection moldings. Part I: Theory and numerical methods. *Polym. Compos.* **1992**, *13*, 317−331.
(41) Advani, S. G.; Tucker, C. L., III The use of tensors to describe and predict fiber orientation in short fiber composites. *J. Rheol.* **1987**, *31*, 751−784.

https://doi.org/10.1021/acsapm.2c00818
ACS Appl. Polym. Mater. XXXX, XXX, XXX−XXX